Mechanical properties of dental investment materials

D. LOW
Discipline of Tooth Conservation, Faculty of Dentistry, The University of Sydney, NSW 2006, Australia
E-mail: dannylow@scientist.com

M. V. SWAIN[1,2]
[1]Biomaterials Science Research Unit, Faculty of Dentistry and [2]Department of Mechanical and Mechatronic Engineering, Faculty of Engineering, The University of Sydney, NSW 2006, Australia

Measurement of the elastic modulus (E) of investment materials has been difficult because of their low strength. However, these values are essential for engineering simulation and there are many methods available to assess the elasticity of materials. The present study compared two different methods with one of the methods being non-destructive in nature and can be used for specimens prepared for other tests. Two different types of investment materials were selected, gypsum-and phosphate-bonded. Method 1 is a traditional three-point bending test. Twelve rectangular bars with dimension of ($70 \times 9 \times 3$ mm) were prepared and placed on supports 56.8 mm apart. The test was conducted at a cross-head speed of 1 mm/min by use of a universal testing machine. The load applied to the test specimen and the corresponding deflection were measured until the specimen fractured. The E value was calculated from a linear part of the stress-strain plot. Method 2 is an ultra micro-indentation system to determine near surface properties of materials with nanometer resolution. The measurement procedure was programd such that the specimens were indented with an initial contact force of 5 mN then followed by a maximum force of 500 mN. Measurement consisted of 10 indentations conducted with a spherical stainless steel indenter ($R = 250\,\mu$m) that were equally spaced (500 μm). The E value rose asymptotically with depth of penetration and would approach the three-point bending test value at approximately four time's maximum contact depth for both materials. Both methods are practical ways of measuring the E of investment materials.

1. Introduction

Dental investment materials are essential in the fabrication of precision dental castings. Generally, two types are employed, depending on the melting range of the alloy. They are the gypsum-bonded and phosphate-bonded investments. Gypsum-bonded investments are the mold materials most commonly employed in the casting of dental gold alloys with liquidus temperatures no higher than 1080 °C. Since these materials have a tendency to decompose at high temperature, phosphate-bonded investments have been used for many years in dentistry for the fabrication of dental castings using high melting-temperature dental alloys (1200–1300 °C) [1].

Both of these materials are brittle cementitious solids with their fracture behavior very similar to heterogeneous materials. Measurement of the elastic modulus (E) value of investment materials has been difficult because of their low strength and to our knowledge no dental studies have been done on the measurement of elastic modulus of these materials. However, these values are essential for engineering numerical simulation [2].

The present study aimed to compare the elastic modulus measurement of investment materials employed by two different methods, in which, one of the methods being non-destructive in nature and can be used for specimens prepared for other tests. This method used an ultra micro-indentation system (UMIS) which determine the near-surface properties of materials with nanometer resolution. Numerous results can be obtained from a small specimen. Fracture behavior of these materials will also be discussed. The other method, namely the conventional three-point bending test maybe used to study the stress-strain behavior, hence calculation of elastic modulus value. It is also possible to measure the fracture behavior of these materials using the three-point bending test.

Correspondence should be addressed to: Danny Low, Biomaterials Science Research Unit, Suite G11, National Innovation Center, Australian Technology Park, Eveleigh, NSW 1430, Australia.

2. Materials and methods

Two commercially available investments were used throughout the study; Cristoquick II (GC Corp., Tokyo, Japan.) (A) and Rematitan Plus (Dentaurum, Pforzheim, Germany) (B). Specifications of investment materials supplied by the manufacturer are listed in Table I. Tap water was used with investment A and a special liquid was supplied with B. The recommended (liquid or water)/powder ratios were 0.33 and 0.16, respectively. Weighing of the liquid and powder was made to an accuracy of 0.01 g (Balance, Type PC 4400, Mettler Instrumente, West Germany). The liquid was dispensed into a mixing vessel without dilution and the investment powder was sifted into the liquid in 15 s. During the next 15 s the powder was fully incorporated into the liquid by hand spatulation at a rate of 3 turns/s. The vessel was assembled within 5 s and mixing was carried out under vacuum at a speed of 425 rpm for 30 s using a mechanical mixer (Combination Unit, Whip-Mix Corp., Louisville, USA). Mixed investment were poured in Teflon molds, covered with Teflon sheet and pressed using a glass slab. Sizes of the molds were $70\,\text{mm} \times 9\,\text{mm} \times 3\,\text{mm}$ for bending test. The investment was allowed to set for two hours from the start of mixing. The prepared specimens were removed from the mold and dried to constant mass for a period of two weeks. Twelve specimens were prepared for each investment. Ambient laboratory conditions during the preparation of investment mixes were $21 \times 1\,^{\circ}\text{C}$ and $50 \pm 10\%$ relative humidity (RH).

2.1. Three-point bending test

The rectangular bar was placed on support 56.8 mm apart and the test was conducted at a crosshead speed of 1 mm/min by use of a universal testing machine (Autograph AG-E, Shimadzu Corp., Kyoto, Japan). The load applied to the test specimen and the corresponding deflection were measured until the specimen fractured. The three-point bend stress and strain were calculated by the following equations [3]:

$$\text{Stress } \sigma \text{ (MPa)} = \frac{3LF}{2WT^2}$$

$$\text{Strain } \varepsilon \text{ (\%)} = \frac{6T\Delta l}{L^2}$$

where L = distance between supports (mm);
F = load (N);
W = width of specimen bar (mm);
T = thickness of specimen bar (mm);
Δl = deflection in bending (mm).

The modulus of elasticity was calculated from the linear portion of the stress-strain plot.

All results were subjected to two sample Student's t-test assuming unequal variances. All statistical analyzes were calculated by a statistical program (Minitab Release 11, 1996, Minitab Inc., USA). Weibull plots were performed on results of the bending test and the Weibull modulus was calculated from the slope of Ln σ and Ln Ln $[1/(1 - P_f)]$ plot, where σ is the bending stress and P_f is the fracture probability. The latter is defined by the relation $P_f = i/(N + 1)$, where i is the rank in strength and N denotes the total number of samples [4].

2.2. Ultra-micro indentation test

The specimen was positioned on the traveling stage of an ultra micro-indentation system (UMIS-2000, CSIRO, Sydney, Australia). Areas to be investigated were displayed on a monitor through a microscope with a $\times 20$ magnification.

The technique employed a spherical indenter having nominal spherical tip of 250 μm radii and adopted the procedure developed by Bell *et al*. [5]. After each selected spot was recorded in a layout file of the operating program (Version 4.0, CSIRO, Sydney, Australia), the traveling stage was translated to the indenting position. The indenter was automatically positioned to the starting spot by the program and then lowered until a contact force of 5 mN (0.5 g) for a maximum measuring force of less than 500 mN (50 g). Measurement consisted of 10 indentations that were equally spaced (500 μm). Upon completion of the measurement the specimen was then automatically translated to the next predetermined indentation spot until all selected spots were measured. The whole system was stabilized in an anti-vibrating chamber and under ambient conditions of $23 \times 1^{\circ}\text{C}$ and $50 \pm 10\%$RH.

The spherical indenter technique, consisting of multiple load/partial-unload cycles unloaded the preceding force by half at each cycle. The elastic and plastic components of indentation were separated and E and mean contact pressure were calculated for each load/partial-unload cycle. Composite elastic modulus (E^*) as a function of indentation depth may be determined by the following equation (when the behavior is entirely elastic)

$$\delta = (9/16)^{1/3}(1/E^*)^{2/3}(1/R)^{1/3}F^{2/3}$$

where δ = total elastic displacement or indentation depth;
R = radius of the spherical indenter;
F = applied force;

TABLE I Specification of investment materials used

Batch number	Cristoquick II (A) 281161	Rematitan Plus (B) powder: 059530 liquid: 119412
W or L/P Ratio	0.33	0.16
Setting time (min)	12	40
Compressive strength (MPa)	4.4	not given

A complete description of this approach is given by Field and Swain [6]. The elastic modulus of the test material (E_m) was then calculated from the following equation

$$1/E^* = (1 - \nu_m{}^2)/E_m + (1 - \nu_i{}^2)/E_i$$

where ν_m is Poisson's ratio of the material and ν_i and E_i is Poisson's ratio and elastic modulus of the indenter, respectively. Poisson's ratios of 0.25 and 0.33 for investment and indenter material, respectively, were adopted for calculation [7].

Mean contact pressure (P_m), synonymous with Meyer's hardness (H_m), was calculated by $P_m(H_m) = F/\pi a^2$ (Fig. 1) and related by $\delta = a^2/R$ for $\delta << R$

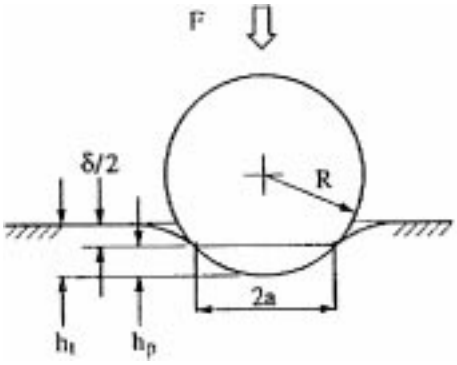

Figure 1 Geometry of the indentation by a spherical indenter at a fully loaded position.

where a = radius of the indentation;
R = radius of the spherical indenter.

A contact or representative stress-strain curve may be obtained by plotting the mean contact pressure (representative stress) against the indentation strain (representative strain = a/R) [5,6].

2.3. Scanning electron microscopy (SEM) observations

SEM observations were made using a scanning electron microscope (Philips SEM XL30) for the indented surface and fracture surface of the three-point bend specimens. Photomicrographs were taken at magnifications of × 1000 and × 2000.

3. Results

The dimensions of specimens prepared for bending test are summarized in Table II and results of bending test are summarized in Table III together with Weibull modulus determined.

At the recommended L/P ratio, the maximum strength of material B is significantly higher than material A ($p < 0.05$). Flexural stress-strain curves of the two materials are shown in Figs 3a and 3b. Material A exhibited catastrophic brittle behavior while material B showed yield-like behavior before the maximum stress and limited strain-softening behavior after the maximum stress. Weibull plots of the maximum bending strengths for both materials are shown in Fig. 4.

Elastic modulus and maximum contact pressure (Meyer's hardness) results obtained from indentation test are summarized in Table IV together with maximum depth of penetration. Meyer's hardness (mean contact pressure) and elastic modulus versus depth of penetration are shown in Figs 5a, 5b, 6a and 6b. Elastic modulus and Meyer's hardness values increased with depth of penetration for both materials. Elastic modulus of material B was significantly higher than A ($p < 0.05$). Besides, elastic modulus of each materials were significantly different between the two method ($p < 0.05$). Four regression models produced from indentation data are shown in Figs 7 and 8. All models indicated were highly significant ($p < 0.001$) and strongly related ($R = 0.99$).

4. Discussion

4.1. Scanning electron microscopy

SEM observations of the indented and fracture surfaces for materials A and B are shown in Figs 2a, 2b, 2c and 2d.

TABLE II Dimensions of rectangular bar for bending test

Materials	Length (mm)	Width (mm)	Thickness (mm)	Mass (g)	Density (kg/m^3)
A	69.45 (0.09)	9.15 (0.01)	3.04 (0.01)	2.77 (0.01)	1431.69 (6.01)
B	69.52 (0.26)	9.12 (0.02)	3.02 (0.01)	4.06 (0.04)	2118.36 (20.75)

TABLE III Results of three-point bending test and Weibull analysis

Materials	Modulus of elasticity (GPa)	Strength (MPa)	Weibull modulus
A	4.41 (0.27)^a	3.90 (0.26)^m	14.48
B	14.66 (0.95)^b	6.84 (0.65)^n	10.38

TABLE IV Results of UMIS test

	Meyer's Hardness (MPa)	Calculated Modulus of elasticity (GPa)	Maximum penetration depth (nm)
A	21.92 (2.29)	3.25 (0.39)^a	15133
B	71.65 (14.87)	11.28 (1.28)^b	4674

Values in brackets are standard deviation. Different suffix denotes that the values are significantly different ($p < 0.05$).

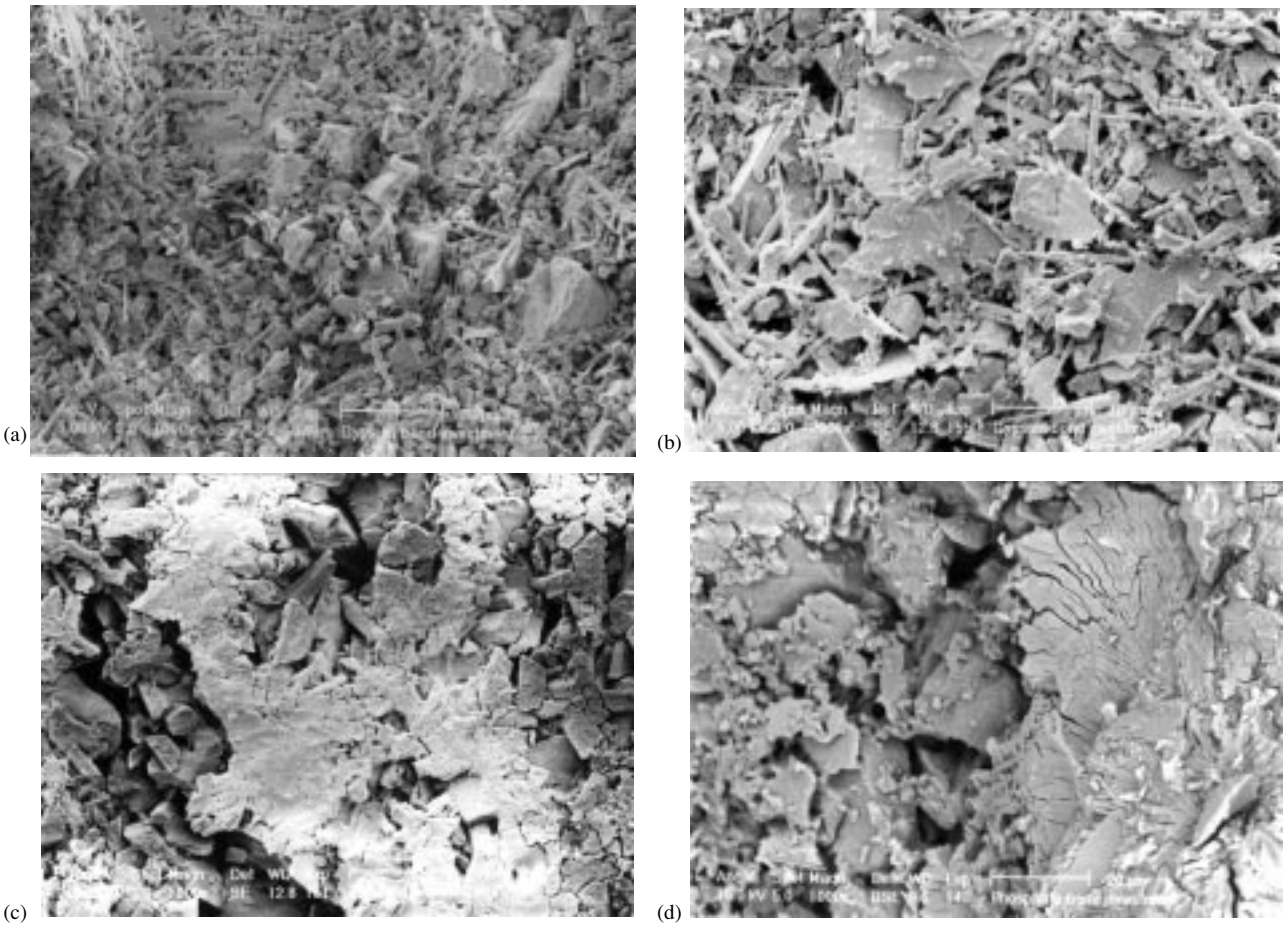

Figure 2 (a) SEM of indented surface of material A. *(b)* SEM of fracture surface of material A *(c)* SEM of indented surface of material B. *(d)* SEM of fracture surface of material B.

These observations show clear differences in the nature of the microstructure. The gypsum-bonded specimen (A) in Figs 2a and 2b shows a fine needle like features of the gypsum crystal bonding coarser particles. There is fine micron sized porosity between the gypsum needles. The vacuum processing lead to no evidence for the large air bubble voids observed by Vekinis *et al*. [10] in their hard mixed batch gypsum specimens.

Material B (Fig. 2c), the phosphate-bonded investment, has a much coarser microstructure with particles 10–20 μm in diameter along with coarser porosity. On the indented surface, there are areas where the phosphate-bonding medium has filled up the space between the particles as well as adjacent poorly bonded regions with large open porosity. The fracture surface of material A (Fig. 2b) is very similar to that of the indented surface, whereas that of material B (Fig. 2d) shows a more fragmented structure. The coarser phosphate-bonding medium indicates very extensive microcracking caused by the fracture event.

4.2. Three-point bending test

Among all the published studies regarding mechanical test of dental investment materials, limited number of flexural tests have been reported. This is probably due to difficulty in specimen preparation. However, flexural tests have many advantages over uniaxial test such as specimen alignment and fixation of specimen to testing machine.

The testing of larger brittle material specimens is more likely to increase the probability of occurrence of defects within the region of tension [4]. Therefore, the test that gives a large area of maximum stress will result in lower strength values for the same material. For instance, a tensile test has lower strength than a bending test specimen of comparable dimensional test. That is, the entire cross-sessional area of the specimen is subjected to the maximum tensile test while only smaller surface area is subjected to the maximum stress in a flexural test. Besides, the size of flaws and position in the material also contribute to strength determination. For example, the probability of the largest flaw being found in the stress-bearing area is higher for tensile test than flexural test and therefore, the strength will be lower. With all these factors in consideration, flexural test appears to be more appropriate for studying stress-strain behavior.

4.2.1. Stress-strain behavior

The lower modulus value of material A (4.41 GPa) than material B (14.66 GPa) indicates that material A would be more susceptible to deformation as only lower stresses would be required for the same amount of strain. This mechanical property is extremely important during setting reaction and thermal behavior of the materials. The fracture strength of material A from the SEM micrographs in Figs 2a and b appears to be controlled by the very fine gypsum needles that bond the coarser particles together. These fine needles would impart a slight degree of crack stability and may

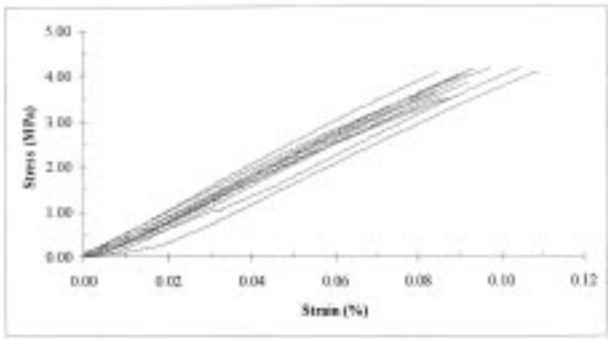

(a)

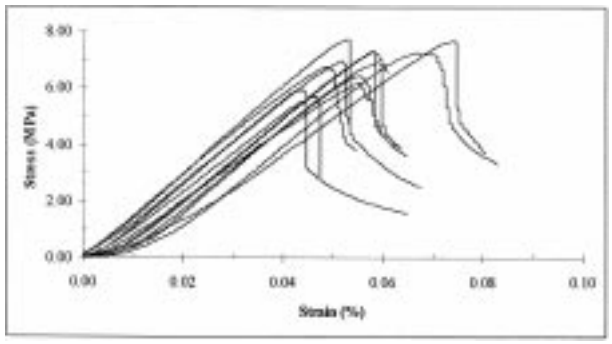

(b)

Figure 3 (a) Flexural stress-strain curves of material A. *(b)* Flexural stress-strain curves of material B.

indicate why this material can sustain a limited plastic deformation prior to catastrophic fracture. The yielding behavior prior to fracture that was demonstrated for material B as compared with A (Figs 3 and 4), suggested that material B could have higher fracture toughness than A. That is, more energy is being absorbed for the initiation and propagation of cracks that were incorporated within the specimen. SEM observations, Fig. 2c shows that this material exhibits very fine cracks and pores throughout the structure. Upon reaching a critical stress, these defects or flaws begin to grow as shown by the slight non-linearity of the stress-strain curve (Fig. 3b). As the applied stress increases, these cracks open through the set material, join together and eventually cause rupture. This stability of the failure process indicates the strain-softening behavior in material B [8]. This behavior is probably due to extensive microcracking and pullout of the coarse particles within the material. The investment material B is typified by the presence of a fracture process zone in which various micro-failure mechanisms take place which is clearly seen in the SEM micrograph in Fig. 2d. Such processes include; micro-cracking, crack deviation, crack branching and interfacial debonding which all contribute to the fracture stability and higher fracture energy.

4.2.2. Weibull analysis

The Weibull modulus is related to the scatter in strength of a brittle material and therefore related to the range of flaw sizes. For example, finding the highest Weibull modulus value is more important than the highest mean strength as the scatter in the strength is reduced [9]. This is particularly so when a study intends to investigate the effect of various factors on the strength because consistent strength data are required for the evaluation. The Weibull moduli value obtained for material A $(m = 14.5)$ in the present study is higher than the value reported for plaster material $(m = 6.2)$ [10]. This may be due to the difference in the water to powder (W/P) ratio, the chemical composition or a consequence of the vacuum processing of the material during investing. On the other hand, the vacuum processing would be expected to remove the larger bubbles and thereby produce a more uniform defect size and hence less scatter of the fracture strength and higher Weibull modulus. The minor difference could be due to the difference in number of specimen [12] and size of specimen [13]. Another aspect of Weibull analysis was the probability of failure at a given stress application. For example, when a specific stress (σ) of 4.1 MPa was applied to material A, the material would have almost 63% probability of failure, whereas material B would have almost zero chance of failure. The Weibull plot enables the relative chance of failure of a material at different stress situations to be determined.

4.3. Ultra-micro indentation test

Compared to the macro three-point bending test, the UMIS test was based on a nano-indentation technique [14–16] in which very small indentations (< 10–20 μm) are produced using loads of milli-newtons. It involves recording the indentation depth rather than the area of the indentation during both loading and unloading of the indenter by a depth sensing apparatus. The UMIS employed in the present study is a computerized controlled nano-indentation machine.

4.3.1. Elastic modulus

Using the UMIS system, the elastic modulus value obtained increased with depth for both materials. There is a logarithmic relationship between depth of indentation penetration and average elastic modulus values of material A and B. The relationships maybe represented by equations of the form, $Y = 0.72\,\mathrm{Ln}(X) - 3.77 (R^2 = 0.98)$ for A and $Y = 2.60\,\mathrm{Ln}(X) - 11.14 (R^2 = 0.98)$ for B. A plot of modulus as a function of penetration depth indicates the influence of the near surface substrate material. The surface roughness and porosity of both materials as seen in

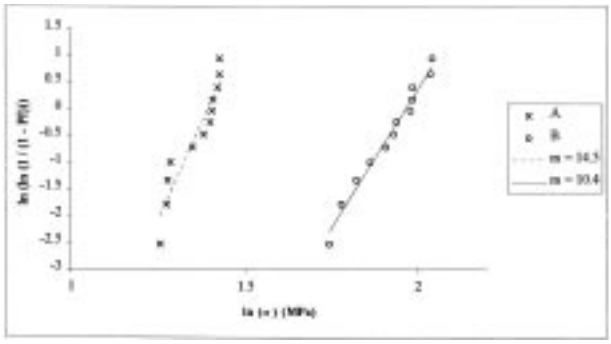

Figure 4 Weibull plot of the bending strength.

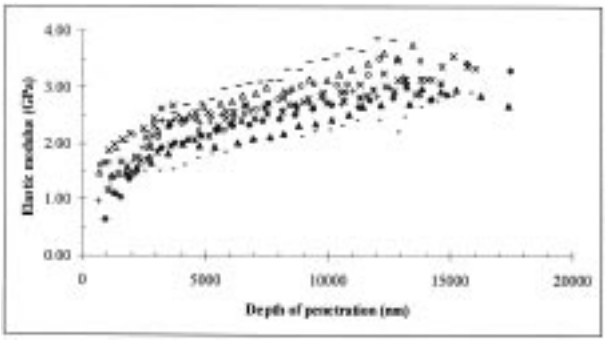

(a)

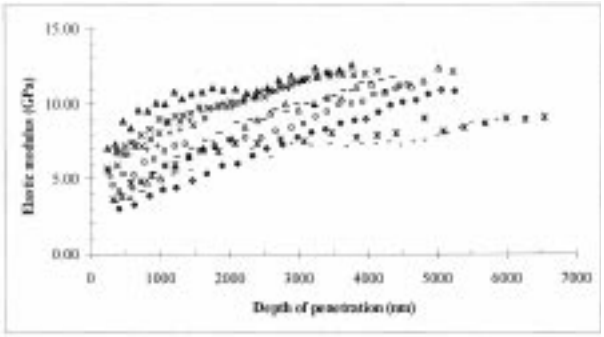

(b)

Figure 5(a) Plot of elastic modulus versus penetration depth for material A. *(b)* Plot of elastic modulus versus penetration depth for material B.

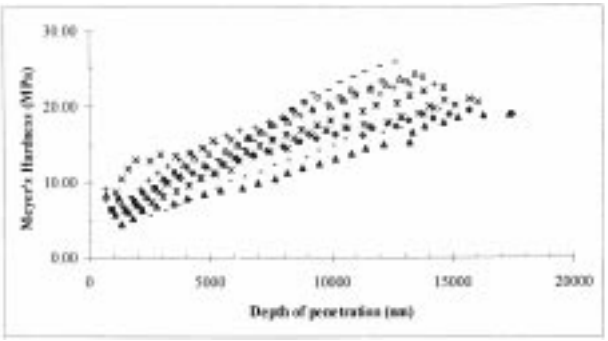

(a)

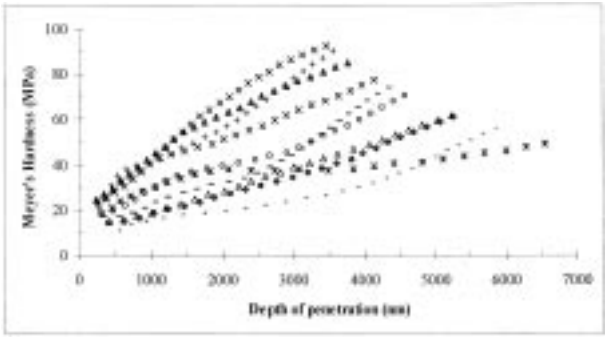

(b)

Figure 6 (a) Plot of Meyer's hardness versus penetration depth for material A. *(b)* Plot of Meyer's hardness versus penetration depth for material B.

Figs 2a and 2c undoubtedly contributes to an initially reduced value of modulus as a consequence of asperity contact with the spherical indenter. Besides, the E value rose asymptotically with depth of penetration and would approach the threepoint bending test value at approximately four times maximum indentation depth measured (that is $\sim 50\,\mu m$ penetration) for both materials as shown in Fig. 7. This is possibly due to packing and densification of small pores and loose debris in both materials.

4.3.2. Meyer's hardness (contact pressure)

The Meyer's hardness or contact pressure values rose with depth of penetration of the indenter because of the initial elastic contact between the sphere and material. Investment materials exhibit inherent porosity on a microscopic scale. In order to have a greater chance of accommodating and hence averaging all components in the material, a larger contact size during a nano-indentation measurement is employed. Vekinis *et al*. [10] reported the mean diameter of porosity was about $212\,\mu m$ for gypsum material. However, with the current vacuum processed materials generate much smaller diameter porosity (Fig 2a and 2b), the diameter of the present indenter ($250\,\mu m$) was considered appropriate. However even these smaller pores would be anticipated to significantly influence the measured values as the contact diameter at maximum load varied from 20 to $90\,\mu m$ for materials B and A respectively.

The Meyer's hardness or contact pressure plots, particularly of material B displayed considerable scatter,

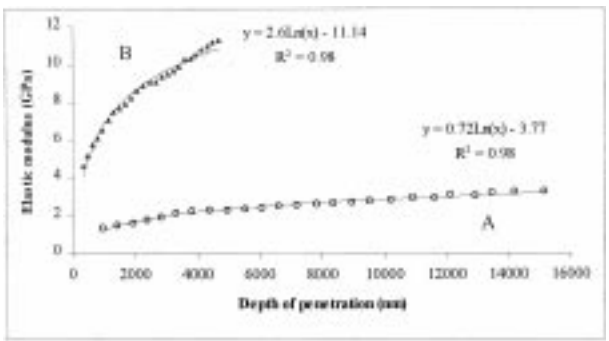

Figure 7 Plot of average elastic modulus versus penetration depth for A and B.

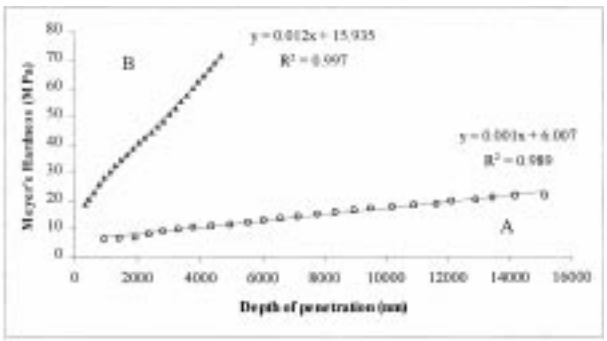

Figure 8 Plot of average Meyer's hardness versus penetration depth for A and B.

although very similar trends. The results rank in the same order as the elastic modulus plots. For the indentations that registered the higher elastic modulus, the contact pressure curves showed almost a linear increase before beginning to rolling over at the maximum contact pressure of 80 MPa. Whereas the lower plots of elastic modulus and contact pressure indicate a discontinuity in the curves undoubtedly associated with cracking or collapsing of the pores.

5. Conclusion

The ability to make elastic modulus measurements of dental investment materials is demonstrated in the present study. In summary, the results obtained from three-point bending test were slightly more consistent than UMIS indentation test. The three-point bending test also enabled Weibull analysis of the fracture stress and some insight of the fracture process of the two materials. The UMIS test had the advantage of providing other information including the hardness, onset of deformation or ''yield'' behavior. Furthermore, the UMIS test provides a more ''local'' measure of modulus whereas three-point bending test is a ''bulk'' value. The SEM micrographs revealed significant differences between the two investment materials which were in accord with the bonding mediums. For material A with its gypsum binder, fine needle like crystals bonded the coarser particles. Whereas for material B a finer phosphate binder that appeared to fragment upon stressing held the much coarser particles together. Microcracking of the binder phase together with the coarser particles in material B were considered responsible for the greater fracture stability of this material.

Acknowledgments

The authors would like to acknowledge Dr Napa Suansuwan for preparation of SEM figures and Mr William Higgs and Mr Ken Tyler for their technical assistance. This study was supported by research grant from the Australian Prosthodontic Society.

References

1. K. J. ANUSAVICE, in ''Phillip's Science of Dental Materials'' (W.B. Saunders Company, Philadelphia, 10th ed., 1996) pp. 471–490.
2. K. ASAOKA and A. TESK, *Dent. Mater. J.* **15** (1996) 121.
3. J. MENCIK, in ''Strength and fracture of glass and ceramics. Glass science and technology vol. 12''(Elsevier, Amsterdam, 1992) pp. 164–168.
4. M. F. ASHBY and D. R. H. JONES, in ''An introduction to microstructures, processing and design'' (Pergamon Press, Oxford, 1st ed., 1986) pp. 169–177.
5. T. J. BELL, A. BENDELI, J. S. FIELD, M. V. SWAIN and E. G. THWAITE, *Metrologia* **28** (1991/1992) 463.
6. J. S. FIELD and M. V. SWAIN, J. Mater. Res. **8** (1993) 297.
7. T. J. BELL, J. S. FIELD and M. V. SWAIN, *Thin. Solid. Films.* **220** (1992) 289.
8. B. COTTERELL and Y. W. MAI, in ''Fracture Mechanics of Cementitious'' Materials (Blackie Academic & Professional, London, 1st ed., 1996) pp. 41–44.
9. J. F. MCCABLE and T. E. CARRICK, *Dent. Mater.* **2** (1986) 139.
10. G. VEKINIS, M. F. ASHBY and P. W. R. BEAUMONT, *J. Mater. Sc.* **28** (1993) 3221.
11. R. V. CURTIS, *J. Dent.* **26** (1998) 251.
12. J. E. RITTER, *Dent. Mater.* **11** (1995) 142.
13. R. A. RODFORD, M. BRADEN and R. L. CLARKE, *Biomater.* **14** (1993) 781.
14. M. F. DOERNER and W. D. NIX, *J. Mater. Res.* **1** (1986) 601.
15. W. C. OLIVER, R. HUTCHINGS and J. B. PETHICA, in ''Microindentation Techniques in Materials Science and Engineering'' (American Society for Testing and Materials, STP 889, Philadelphia, 1986) pp. 90–108.
16. G. WILLEMS, J. P. CELIS, P. LAMBRECHTS, M. BRAEM and G. VANHERLE, *J. Biomed. Mater. Res.* **27** (1993) 747.
17. J. S. FIELD and M. V. SWAIN, *J. Mater. Res.* **10** (1995) 101.

Received 1 October 1999
and accepted 13 December 1999